Original Article	*Curr. Appl. Sci.*, **2023**, *1*(1):35-50 DOI: 10.22034/cas.2021.144387	Current Applied Sciences

Investigation and Comparison of Band Gap for Photon Crystals by Wave-Plate Method with Different Backgrounds

Fardin Sadeghfar

Department of Physics, University of Zanjan, Zanjan 45371-38791, Iran

Corresponding author's e-mail: *Fardin_1942@yahoo.com*

Article Information

Received: 10 December 2022
Revised: 14 January 2023
Accepted: 27 January 2023
Published online: 05 February 2023

Keywords

Wave-plate method
Band gap
Photon crystals
Different backgrounds

Abstract

Hexagonal photon crystal structure with seven nanorods on each side where the rods are arranged in air and with a triangular arrangement was studied. The structure has a symmetry, and each rod can be repeated in any direction, and the unit cell in two dimensions of the surface contains two basic vectors and is actually the smallest component in terms of surface which can be reconstructed and repeated to reconstruct the whole photon crystal. Usually, the simplest selection for a triangular photon crystal is a rhombus with sides equal to the lattice constant (a = 0.5 μm). The plate wave development method by energy band simulation of two-dimensional photonic crystals using RSOFT software has been proposed. The RSoft is the core program in the RSoft Photonics Suite and acts as a control program for RSoft's passive. Photonic crystals, Zinc Oxide, Silicon and Zinc Oxide - Silicon by different refractive index (hazardous toxic gases) and air were considered as background. The full band gap and wavelengths that do not allow photon crystals to enter were determined. Also, the correlation spectrum and the wavelength transmission direction with different relative power for each photon crystal were determined.

1. Introduction

Recently, many research has been done on photon crystals for different kinds of optical devices that have great potential to be used as the main platform for design and implementation [1-10]. Photonic crystals are inhomogeneous dielectric media by periodic variation of the refractive index and constituted by a periodic repetition of inclusions in a matrix background, which has received much attention during the recently [11]. In general, photonic crystals have a photonic band gap. That is the range of frequencies in which light cannot propagate through the structure. Photonic crystals [12, 13], are artificially created materials that are able to represent a photon band gap; that is, they do with photons what a normal semiconductor does with electrons, a

state in which photons with certain energies cannot propagate inside the crystal, regardless of polarization and propagation direction. Therefore, the photon band gap is probably the true optical analog of the fundamental gap of a semiconductor. Since they were invented in 1987, photon crystals have attracted considerable attention due to their unusual optical properties. The unique photon crystal properties also mean that they are now recognized as a novel and fundamental field in optoelectronics. Silicon is an excellent model system in order to study the optical properties of two-dimensional photonic crystals, and macro-porous silicon with high dielectric contrast, very high aspect ratio and full compatibility with the microelectronics industry. It also has several unique applications in many other fields such as electronics, micromachining, gas measurement, and biotechnology. Research on silicon is constantly evolving because of its enormous potential for applications. Photonics, the photons technology, arose out of the advent of lasers and the optical fibers, which are the best choice as source and channel of the information carrier: light particles (or photons). Photons have several advantages over electrons. They travel in a dielectric material at much higher speeds than electrons in a metallic wire. The fiber-optic cables that today span the ocean, are good for long hauls. Today, optical interconnects through optical fibers are already used to connect different computers [14-17]. Investigation of photonic crystals has become one of the modern rapidly developing directions [18-20]. Photonic crystal, the refractive index is modulated at wavelength scale, a lot of interesting applications in different domains [21, 22]. In the case of photonic crystals, it requires that the refractive indices contrast should be as high as possible. Some photonic crystals are made by polystyrenes or SiO_2 nanoparticles [23-26]. The possibility of absolute band gaps in their band structure, these materials have found several potential applications, in particular in the wave guiding field and filtering [27] as well as in the field of sound isolation [28]. When the periodicity extends over all three dimensions and if the dielectric contrast is high enough, the stop gaps in all directions can overlap to form a complete photonic band gap (PBG); that is, a frequencies range for which light propagation is forbidden, irrespective of the direction of propagation. The photonic band gap might therefore be the true optical analogue of the fundamental band gap of a semiconductor [29]. The photonic band gap makes it possible for photonic crystals to act as optical passive devices. As was first put forward [29], the photonic band gap may completely show spontaneous emission. Excited atoms in a photonic crystal with their transition frequencies tuned to the band gap cannot emit photons, because inside the gap there are no quantum mechanical states available into which photons can go. It has been demonstrated that spontaneous emission is inhibited in a microwave region by surrounding the atoms by a pair of metal plates [30]. The existence of band gaps and confined modes has especially been investigated in photonic crystal slabs [31, 32] and more lately in photonic crystal slabs [33-37] in particular in view of the technological realization of integrated structures in order to electronics and telecommunications. The PBG depends upon the arrangement and shape of elements of the photonic crystal, fill factor, and dielectric contrast of the two mediums used in forming photonic crystal. The most vital feature of photonic crystals is the capability to support spatially electromagnetic localized modes when a perfectly periodic photonic crystal has spatial defects [38-40].

2. Materials and Methods

2.1 *Viewing the mode spectrum*

The correlation method uses the FFT of a correlation function to calculate the state spectra, to determine the states that support a structure. There are several state-of-the-art BPM solutions developed. The first case is the correlation method and is used to calculate the states and properties of the multistate scattering [41]. Recently, a technique

called imaginary distance BPM has been developed [42, 43]. It should be noted that the imaginary distance BPM of this method is formally equivalent to many other state repetition solving methods [44, 45]. BPM-based problem solving is a random field given to a geometry. Z-same is done, a kind of BPM emission. Since the structure is uniform along Z, the diffusion can be described equally in terms of diffusion modes and constants, and the structure can be given a random $\emptyset_{in}$(x) random field for 2D diffusion from a scalable field for simplicity. A state of the structure is extended as

$$\emptyset_{in}(x) = \sum_m C_m \emptyset_m(x). \quad (1)$$

This set, of course, must contain a true summary of the guided states and the reintegration of the radiation state. Propagation through the structure can be expressed as follows:

$$\emptyset\ (x\ ,\ z) = \sum_m C_m \emptyset_m(x)\ e^{i\beta_m z} \quad (2)$$

In any BPM-based state solution technique, the propagation field obtained through BPM is a concept for determining how to extract state information from BPM equivalent to the results of the above expression. As the name implies, at the imaginary distance of BPM, the longitudinal coordinates of Z are replaced by Z '= iZ, so propagation along this imaginary axis must be followed.

$$\emptyset\ (x\ ,\ z^{'}) = \sum_m C_m \emptyset_m(x)\ e^{\beta_m z^{'}} \quad (3)$$

The growth rate of each state is equal to its true propagation. The basic idea of the working method is to set up a custom field, say a Gaussian, and spread the field through the structure along an imaginary axis. Since the ground state (m = 0) has the highest emission by definition and it is proved that its share in this field has the highest growth rate and after a certain distance will dominate the others. Just put the background pattern Q_0(x), then the propagation constant can be obtained with the following variable expression:

$$\beta^2 = \frac{\int \emptyset^*(\frac{\partial^2 \emptyset}{\partial x^2} + k^2 \emptyset) dx}{\int \emptyset^* \emptyset dx} \quad (4)$$

The higher-order modes can be obtained using an orthogonalization method to reduce contributions from lower-order modes when publishing [46]. It eliminates the error given that we have solved for the paraxial eigenvalues, and it is important to note that the imaginary distance of BPM from the usual technique, performing a standard propagation and waiting for the solution to reach a steady state, is not the same. In the correlation method, an arbitrary field is launched into the structure and propagated through normal BPM during propagation. The following correlation function is calculated between the input part and the field of the advertising.

$$P(z) = \int \emptyset_{in}^*(x) \emptyset(x, z) dx \quad (5)$$

Using Equations (1) and (2), the correlation function can also be expressed as follows:

$$P(z) = \sum_m |C_m|^2\ e^{i\beta_m z} \quad (6)$$

From this statement, it can be deduced that a Fourier transform of the calculated correlation function must have a spectrum with peaks at certain diffusion constants. The relevant fields are obtained by the second propagation by the propagation field pulse versus the known propagation to the constant through the following equation:

$$\emptyset_m(\mathrm{x}) = \frac{1}{L}\int_0^L \emptyset(x\ , z)\, e^{-i\beta_m z} \qquad (7)$$

Several modifications can be made to the diffusion constants: First, a modification is made that takes in to account the error created by solving the paraxial equation, not the exact Helmholtz equation. More details can be found in the reference [41]. Second, by degrading the state, one can find the imaginary part of the constant propagation and the properties in the wave equation and the solution for the constant propagation. This not only results in an imaginary value, but is also a modified real value. The basic mode of the simple waveguide is a screen whose propagation constant is displayed above this calculated mode, the imaginary complex effective coefficient indicating the disappearance of the mode. The state calculation can be done with the simulated curvature features off (straight waveguide). During the simulation, there are actually two types of simulations. While the correlation method is generally slower than the imaginary distance BPM, it has the advantage that it is sometimes applicable to problems that are difficult or impossible for imaginary distance BPM, such as leaky or radiating modes.

2.2 *Simulation method*

The model made by the RSOFT software is shown (as in Figure 1). Only in the present model, different backgrounds were used. The refractive index of Air, Zinc Oxide, Silicon and Zinc Oxide - Silicon are 1, 2.4, 3.78, and 3.366, respectively, and the bars diameter is 0.2 μm and the lattice constant is 0.5 μm. Here, the calculations of a transmission spectrum for several finite photon crystal lattices with different backgrounds are discussed. Several band gaps are found in one direction of propagation in crystals. As shown in the figure below, the Photonic Band Gap (PBG) lattice contains a 2D triangular array with a dielectric structure with the refractive index described above. The simulation range is chosen along Z and a constant along X. Two fields one on the left (X, Z) = (-2.5, 0) and the other on the right of the structure (X, Z) = (2.5, 0) and also a monitor on the right (X, Z) = (2.5, 0) are installed in order to record the electric fields passing through the photonic crystal. Boundary conditions are periodically along X and perfectly matched layer (PML) along Z. This configuration shows that a finite structure is being simulated. A monitor is created to record the transmitted field on one side of the structure. Frequency analysis options for this monitor are set to FFT to calculate the spectra, and the stop time is set to 100. After completing the simulation, more energy will leave the domain field. In each case several band gaps are clearly visible.

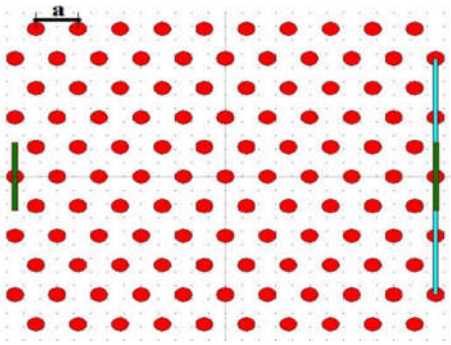

Figure 1. Schematic of the crystal structure

3. Results and Discussion

As can be seen from the scattering curves (as in Figure 2), the photon crystal bond structure for the TE mode of Zinc Oxide and Silicon and Zinc Oxide-Silicon nanostructures is available, and it is observed that there is a complete band gap. The full band gap prevents the propagation of waves at certain frequencies. Reflects a wave reflected to a two-dimensional photon crystal. The set of crystal atoms can be considered as a mirror by non-zero reflection coefficients for the reflected wave. Partial reflections of each surface can lead to a full reflection of the wave in the direction of its snell reflection if the amplitude of each phase is amplified. To amplify the phase, the difference in the path shown must be a multiple of the wavelength, (e.g., $2d\cos\theta = m\lambda$), and this condition is a Bragg reflection. In this way, some waves with wavelengths pass through a specific direction and others reflect, shown as in Table 1. Therefore, the frequencies that strike the crystal in the band gap region are reflected, i.e., these frequencies are not allowed to enter the environment, which is calculated according to the formula ($\omega = a / \lambda$), where a is the lattice constant, λ is the wavelength, and ω is the wave frequency. And also, it shows the refractive index *n* of different materials. As you can see in Figure 1, as well as from the results in Table 1, increasing the refractive index reduces the input frequency at the full band gap in nanostructures. Also, in some nanostructures such as Silicon and Zinc Oxide-Silicon, which had two complete bond gaps in the scattering curve, one of the bond gaps disappeared by increasing the refractive index. This means that with the disappearance of the band gap, the wavelength is allowed to enter the environment of the nanostructures. In general, decreasing and increasing the refractive index cause disruption in the environment of nanostructures. It should be noted that the refractive index was changed by changing the air background to hazardous and toxic gases in Table 1.

According to the conditions created and the results obtained (as in Figure 2 and Table 1), these results can be described as follows. The reflective refractive index is a parameter to control the intensity of the Fresnel effect from the corner to the center of the material. A schematic for better understanding of the situation is shown (as in Figure 3).

According to the results obtained (as in Table 2) and using the equation ($\omega = a / \lambda$), it is possible to calculate the wavelengths that are not allowed to enter the structures, (e.g., in the area of the full band gap). As we can see in Figure 4, the monitor value is shown in terms of different wavelengths and the recorded spectrum is shown on two monitors (the blue spectrum on the left of the monitor, e.g., the location of the electric field emission, and the green spectrum on the right side of the structure). As you can see in the green spectrum, where the lines go to zero and in the specified wavelength range the value recorded on the monitor is zero, it is defined as the forbidden band, which is placed by placing the wavelengths in the equation ($\omega = a / \lambda$) and concludes that it corresponds to the frequencies expressed (as in Table 1 and Figure 2). With both simulation methods, wavelengths located in the full band gap region can be identified. The complete band gap can also be obtained using the equation ($Eg = hc/\lambda$) . In Table 2, it is shown the energy (E^v-E^c) and wavelengths (λ^v- λ^c) between the last capacitance band to the first conduction band, which are not allowed to enter the structures between these intervals.

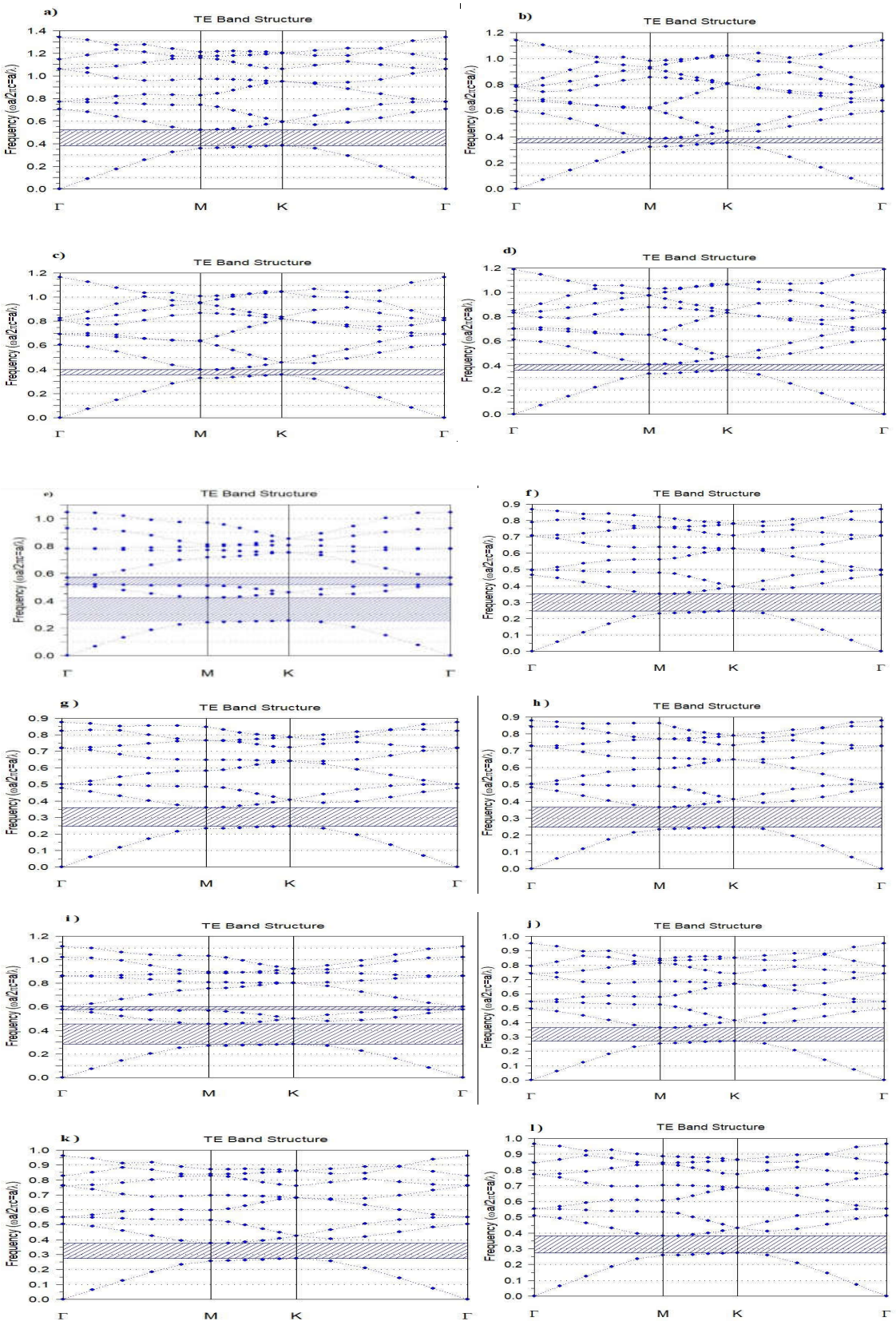

Figure 2. Strip structures a, b, c and d) Zinc Oxide e, f, g and h) silicon i, j, k, and l) Zinc Oxide -silicon, respectively for Air, NO_2, C_8H_{18} and C_6H_{16} background

Table 1. Frequencies obtained by changing the refractive index by changing the background with a lattice constant μm a = 0.5

Materials	**N**			a/λ
Background	**Refractive index**	**Zinc Oxide**	**Silicon**	**Zinc Oxide - Silicon**
Air	1.0	0.38-0.51	0.25-0.42	0.28-0.45
			0.51-0.56	0.57-0.6
NO	1.0002697	0.38-0.52	0.25-0.42	0.28-0.45
			0.51-0.57	0.57-0.6
NO_2	1.449	0.351-0.38	0.245-0.35	0.27-0.36
H_2S	1.000644	0.38-0.52	0.25-0.42	0.28-0.45
			0.51-0.57	0.57-0.6
NH_3	1.3327	0.36-0.41	0.245-0.37	0.27-0.38
CH_4	1.0004365	0.38-0.52	0.25-0.42	0.28-0.45
			0.51-0.57	0.57-0.6
C_2H_6	1.0007483	0.38-0.52	0.25-0.42	0.28-0.45
			0.51-0.57	0.57-0.6
C_5H_{12}	1.3570	0.36-0.41	0.245-0.365	0.27-0.38
C_6H_{16}	1.3529	0.36-0.41	0.245-0.365	0.27-0.38
C_7H_{16}	1.3872	0.355-0.39	0.245-0.36	0.27-0.37
C_8H_{18}	1.3972	0.355-0.39	0.245-0.36	0.27-0.37
C_2H_2	1.00056142	0.38-0.52	0.25-0.42	0.28-0.45
			0.51-0.57	0.57-0.6

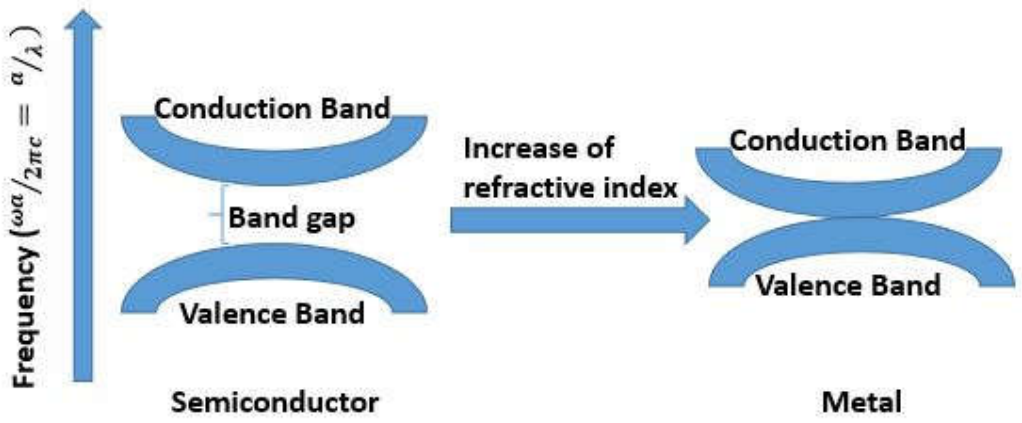

Figure 3. Schematic of the process of changing photon crystals

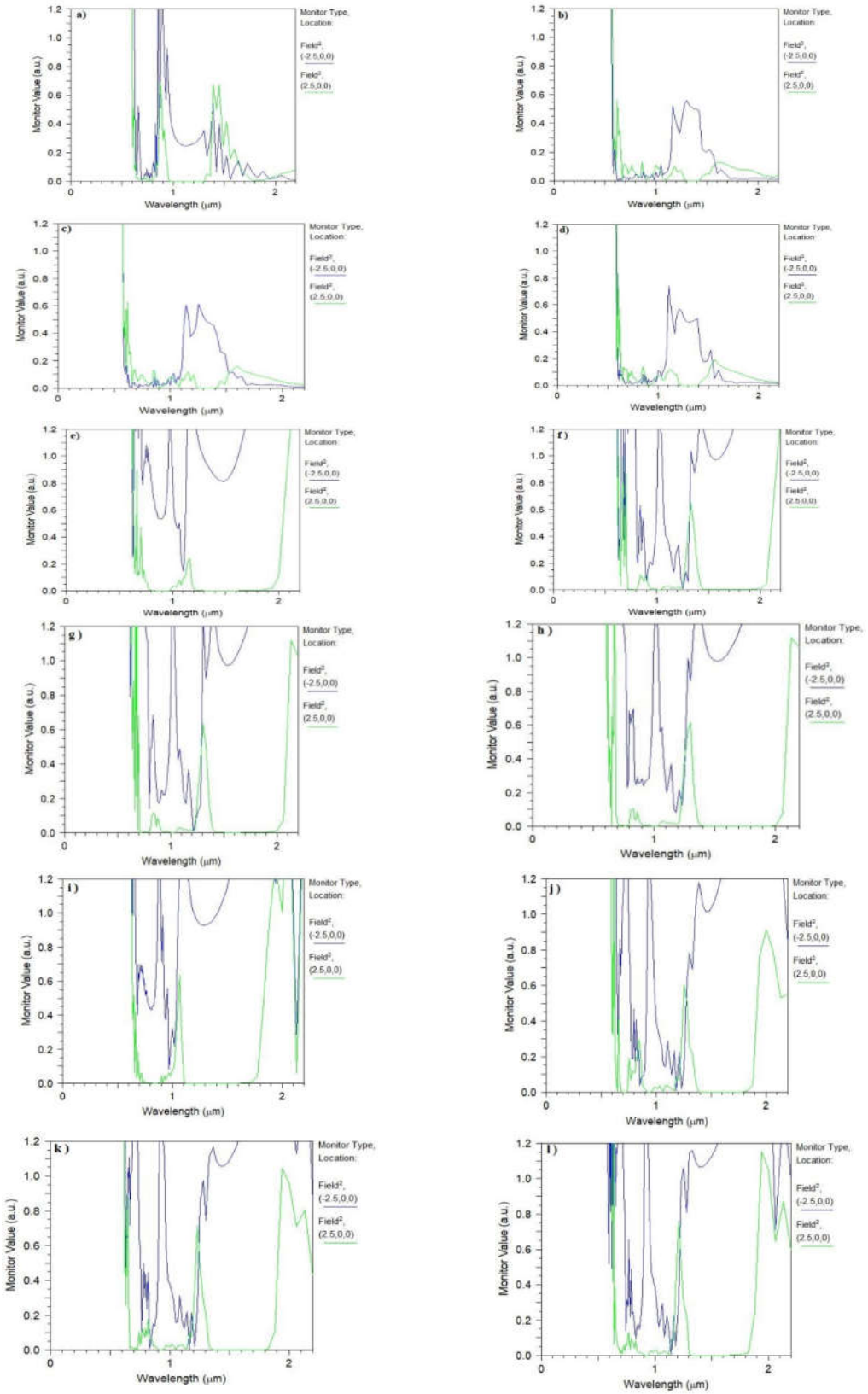

Figure 4. Determination of full band gap for photon crystals: a, b, c and d) Zinc Oxide e, f, g and h) silicon i, j, k and l) Zinc Oxide -silicon, for Air, NO_2, C_8H_{18} and C_6H_{16} background, respectively.

Table 2. Results of changing the refractive index by changing the background with a lattice constant a = 0.5 µm

Materials background	Zinc Oxide			Silicon			Zinc Oxide - Silicon		
	E^v (nm)	E^c (nm)	λ^v- λ^c (µm)	E^v (nm)	E^c (nm)	λ^v- λ^c (µm)	E^v (nm)	E^c (nm)	λ^v- λ^c (µm)
Air	0.94	1.26	1.31-0.98	0.62	1.04	0.2-1.19	0.69	1.1	1.78-1.1
				1.26	1.38	0.98-0.89	1.4	1.48	0.87-0.83
NO	0.94	1.29	1.31-0.96	0.62	1.04	0.2-1.19	0.69	1.1	1.78-1.1
				1.26	1.41	0.98-0.87	1.4	1.48	0.87-0.83
NO_2	0.87	0.94	1.42-1.31	0.6	0.86	2.04-1.42	0.67	0.89	1.85-1.38
H_2S	0.94	1.29	1.31-0.96	0.62	1.04	0.2-1.19	0.69	1.1	1.78-1.1
				1.26	1.41	0.98-0.87	1.4	1.48	0.87-0.83
NH_3	0.89	1.01	1.38-1.21	0.6	0.91	2.04-1.35	0.67	0.94	1.85-1.31
CH_4	0.94	1.29	1.31-0.96	0.62	1.04	0.2-1.19	0.69	1.1	1.78-1.1
				1.26	1.41	0.98-0.87	1.4	1.48	0.87-0.83
C_2H_6	0.94	1.29	1.31-0.96	0.62	1.04	0.2-1.19	0.69	1.1	1.78-1.1
				1.26	1.41	0.98-0.87	1.4	1.48	0.87-0.83
C_5H_{12}	0.89	1.01	1.38-1.21	0.6	0.9	2.04-1.36	0.67	0.94	1.85-1.31
$C6H_{16}$	0.89	1.01	1.38-1.21	0.6	0.9	2.04-1.36	0.67	0.94	1.85-1.31
$C7H_{16}$	0.88	0.96	1.4-1.28	0.6	0.89	2.04-1.38	0.67	0.91	1.85-1.35
C_8H_{18}	0.88	0.96	1.4-1.28	0.6	0.89	2.04-1.38	0.67	0.91	1.85-1.35
C_2H_2	0.94	1.29	1.31-0.96	0.62	1.04	0.2-1.19	0.69	1.1	1.78-1.1
				1.26	1.41	0.98-0.87	1.4	1.48	0.87-0.83

The first mode calculates the effective coefficient values, the second cross-section calculates and finds the effective coefficient mode. Unlike the iterative method, it is related to an imaginary effective coefficient that is displayed by the simulation results. Mode number (m = 0) and effective (n_{eff}) coefficient are displayed in the upper right corner of each graph. All these measurements are for the TE mode. This method is mostly used for transmission analysis. The real and imaginary part of the effective refractive index of structures is shown as a function of the lattice constant filling ratio of (500 nm) and the wavelength of (1100 nm) that we considered for these structures. As you can see (in Figure 5), the gauge for the state number (m = 0) for the TE state for the Zinc Oxide structure is different from the Silicon structure, but by combining them, Zinc Oxide-Silicon has no change in diffusion direction and effective coefficient for the (m = 0) state, was not created. From these results, it can be concluded that the highest cross-sectional share for transmission for Zinc Oxide-Silicon structure is related to Silicon.

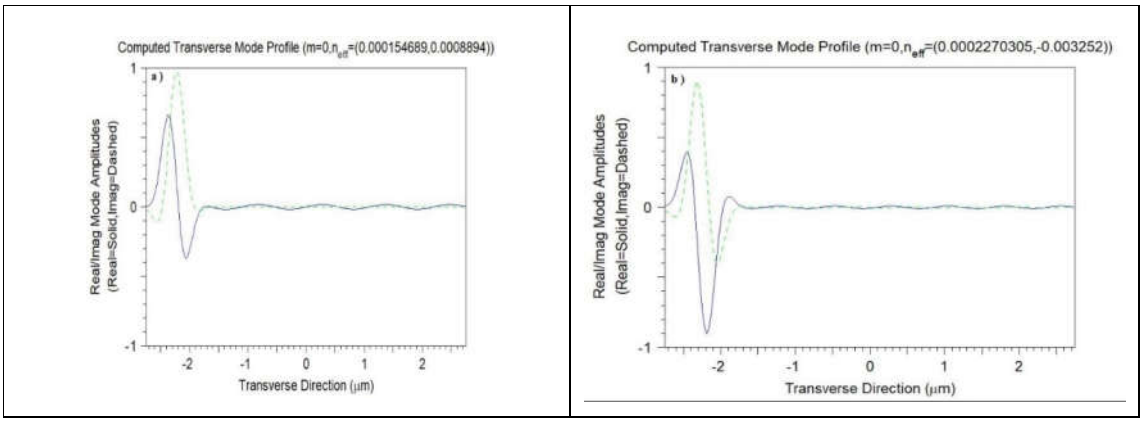

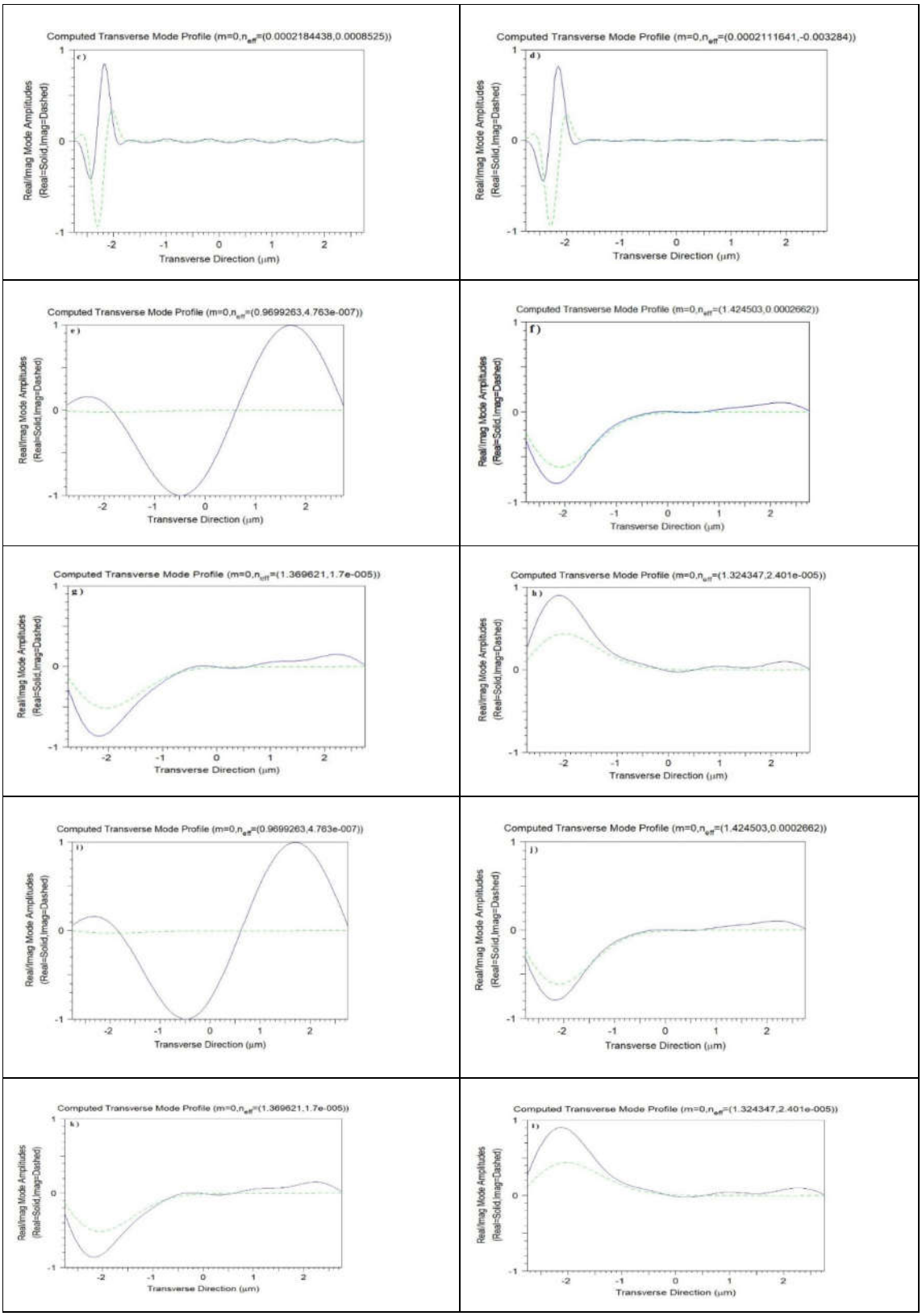

Figure 5. Calculation mode for the positive curvature radius of the plane waveguide: a, b, c and d) Zinc Oxide structure e, f, g and h) Silicon structure i, j, k and l) Zinc Oxide -silicon structure, for Air, NO_2, C_8H_{18} and C_6H_{16} background, respectively

The like any discipline, there are a number of concepts in the study of photon devices. The correlation method uses FFT, a correlation function, to calculate the state spectrum. To determine the modes that a structure supports. The 2D structure (on XZ plane) with TE mode with E_y field and imaginary refractive index units is considered as follows. ($n_{imag} = {}^{\gamma\lambda}/_{4\pi}$), λ is the wavelength, γ is the exponential loss coefficient defined in such a way that the power to determine decays is expressed as ($e^{-\gamma z}$) and in units (μm^{-1}). Using the results of the Fourier transform from the calculation of the (m = 0) mode, only one mode is found, which is described to the right of the graphs for each structure ((m, Δn_{eff}, %weight) and n_{bar}). These results rely on the Fourier transform. The propagation lengths were considered the same for all the structures you see (as in Figure 6), and the peaks of the (m = 0) mode spectrum are well defined. The solution of the mode is to select peaks that are above a certain threshold in the solid state spectrum scheme. In this simulation, the values of (n_{eff}) min and (n_{eff}) max can be adjusted due to the wide range of effective coefficients found by the state solution, but in this simulation, it was considered by default. Also (n_{eff}) log output of the effective coefficient values during an iterative mode calculation can be useful for studying convergence. The (n_{eff} - n_{bar}) parameter indicates the number of data points in the frequency direction, (n_{bar}) is the reference refractive index.

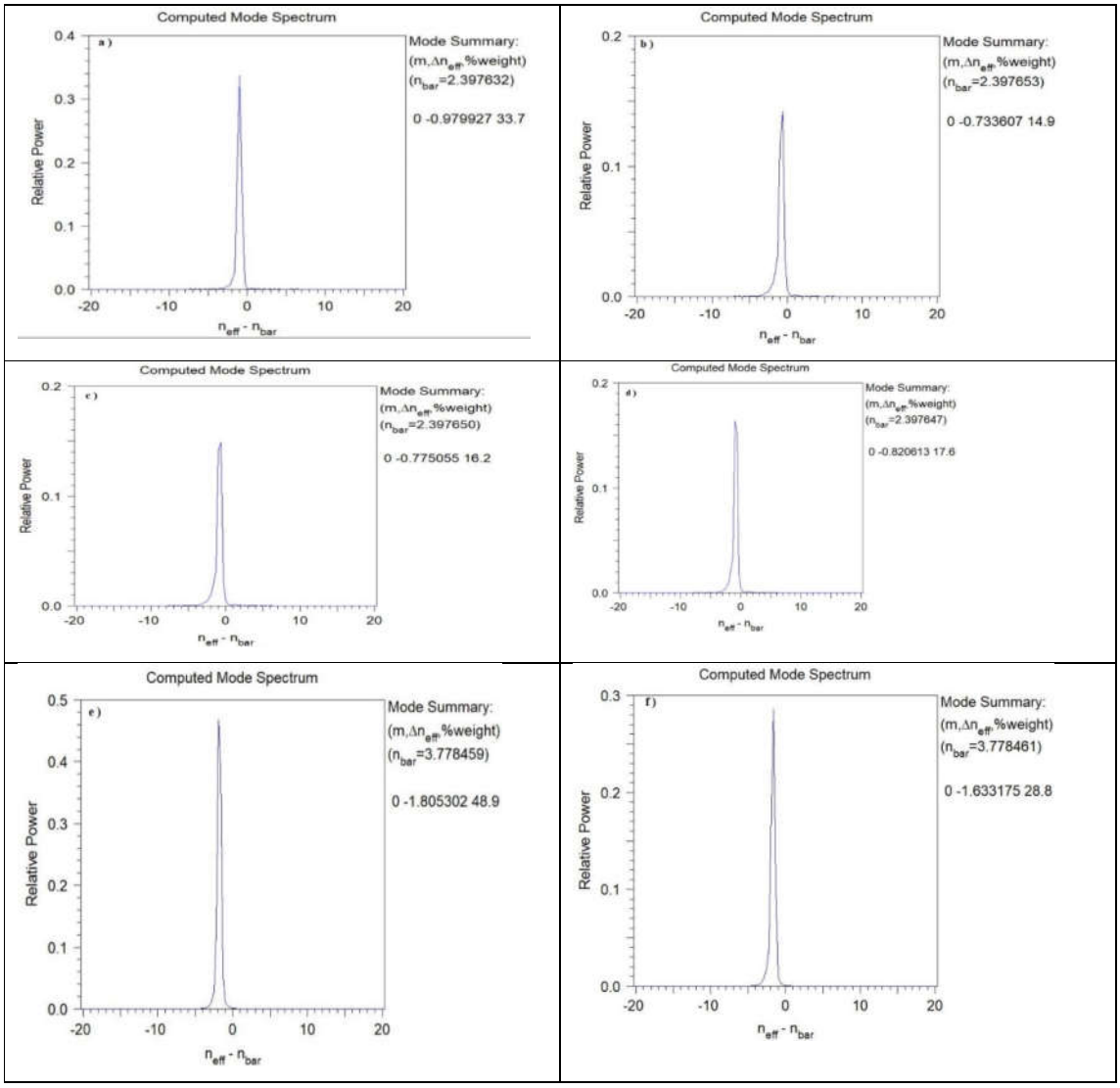

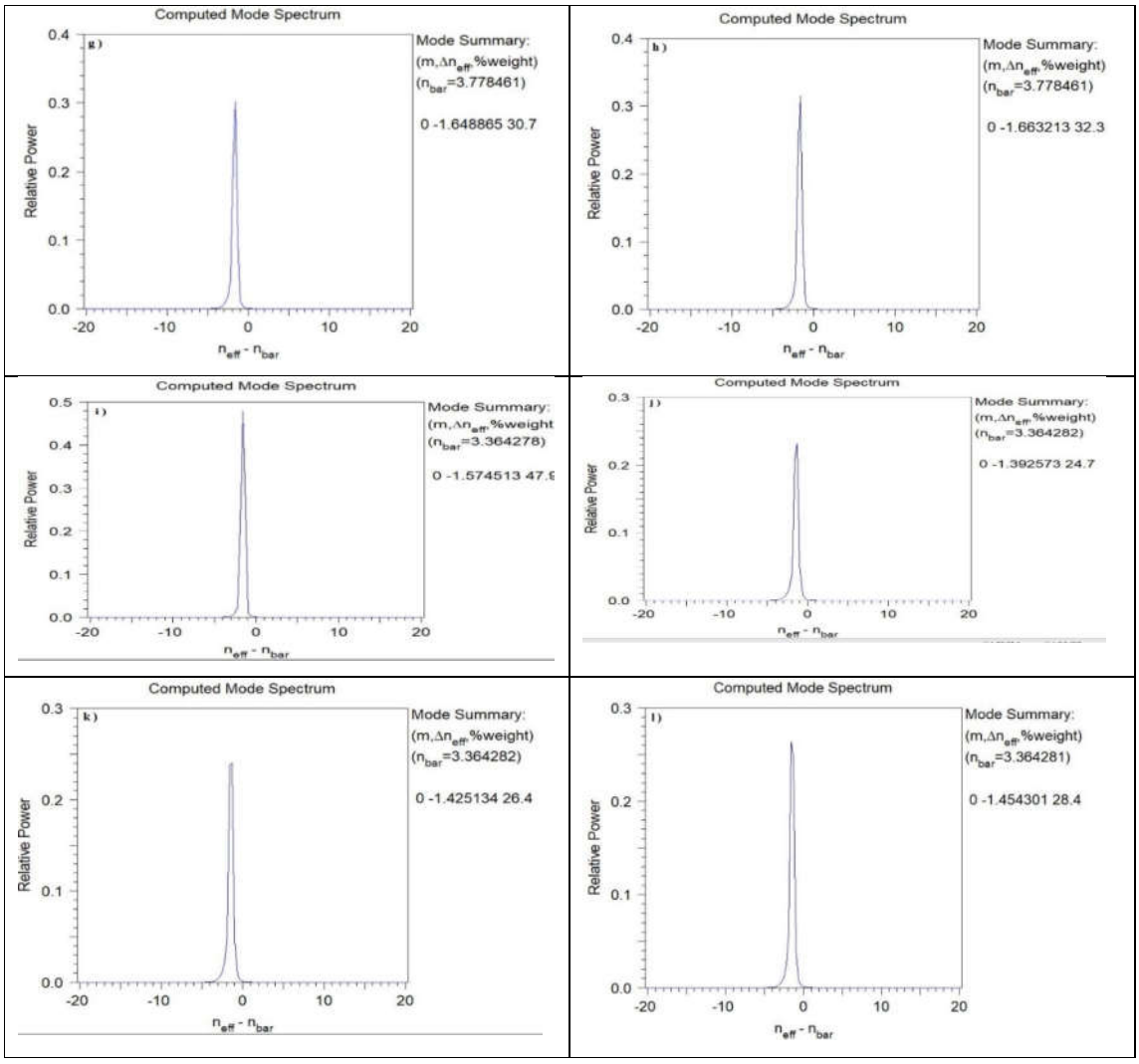

Figure 6. The Fourier transform results from the calculation of the state of photon crystals: a, b, c and d) Zinc Oxide, f, g and h) silicon I, j, k and l) and Zinc Oxide -silicon, for Air, NO_2, C_8H_{18} and C_6H_{16} background, respectively

4. Conclusions

The Zinc Oxide, Silicon, and Zinc Oxide-Silicon photon crystals with different refractive indices (hazardous toxic gases) and air are very useful as a background. Because of creating a change in crystal structure and using gases as a background, it maintains its crystal structure and can be used as a dielectric. These crystals were complete band gaps with a change in the background, and none of the crystals were driven to the metallic state only by changing the refractive index, but retained their original state as a dielectric. In this simulation, the semiconductor structure is moved to the metal structure by increasing the refractive index. In this simulation, frequencies and wavelengths that were not allowed to enter the photon crystal were detected. The amount of energy was determined for the highest valence layer (E^v) and the lowest conduction layer (E^c) for each structure, and it was found that by increasing the refractive index, the amount of full band gap between the structures decreased. Also, the correlation spectrum and the direction of wavelength transmission with different relative power for each photon crystal were different by changing the structure with different backgrounds for Silicon and Zinc Oxide, but with Silicon-Zinc

Oxide combination, the correlation spectrum was similar to Silicon and this showed that Silicon has a greater role in transmitting wavelengths. A simple iteration method allows a self-consistent solution to be designed for such systems. The design of these systems is useful for gas detection and sensitivity. It is possible to identify wavelengths that are not allowed to enter the designed system.

Conflicts of Interest

The authors declare that there are no conflicts of interest regarding this article.

References

1. John S. Strong localization of photons in certain disordered dielectric superlattices. *Phys. Rev. Lett.*, 1987, 58(23):2486.

2. Ren C, Wang P, Cheng L, Feng S, Gan L, Li Z. Multichannel W3 Y-branch filter in a two dimensional triangular-lattice photonic crystal slab. *Optik*, 2014, 125(24):7203-7206.

3. Kannaiyan V, Savarimuthu R, Dhamodharan S. Investigation of 2D-photonic crystal resonant cavity based WDM demultiplexer. *Opto-Electron. Rev.*, 2018, 26(2):108-15.

4. Fedaouche A, Badaoui HA, Abri M. An ultra-compact 1× 5 and 1× 10 beam-splitters in photonic crystal slab. *Optik*, 2018, 157:1300-1305.

5. Moungar A, Badaoui H, Abri M. 16-Channels wavelength efficient demultiplexing around 1.31/1.55 µm in 2D photonic crystal slab. *Optik*, 2019, 193:162685.

6. Askarian A, Akbarizadeh G, Fartash M. An all-optical half subtractor based on Kerr effect and photonic crystals. *Optik*, 2020, 207:164424.

7. Yang J, Zhu Z, Feng J, Xue M, Meng Z, Qiu L, Mbola NM. Dimethyl sulfoxide infiltrated photonic crystals for gas sensing. *Microchem. J.*, 2020, 157:105074.

8. Samoi E, Benezra Y, Malka D. An ultracompact 3× 1 MMI power-combiner based on Si slot-waveguide structures. *Photonics Nanostruct.*, 2020, 39:100780.

9. Maleki M, Mir A, Soroosh M. Design and analysis of a new compact all-optical full-adder based on photonic crystals. *Optik*, 2021, 227:166107.

10. Boufenar R, Bouamar M, Hocini A. Numerical analysis of a temperature sensor based on the photonic band gap effect in a photonic crystal fiber. *Chin. J. Phys.*, 2018, 56(3):1126-1132.

11. Pennec Y, Rouhani BD, El Boudouti E, Li C, El Hassouani Y, Vasseur J, Papanikolaou N, Benchabane S, Laude V, Martinez A. Simultaneous existence of phononic and photonic band gaps in periodic crystal slabs. *Opt. express*, 2010, 18(13):14301-14310.

12. Yablonovitch E. Photonic band-gap structures. *J. Opt. Soc. Am. B*, 1993, 10(2):283-295.

13. Krauss TF, Richard M, Brand S. Two-dimensional photonic-bandgap structures operating at near-infrared wavelengths. *Nature*, 1996, 383(6602):699-702.

14. Bardeen J, Brattain WH. The transistor, a semi-conductor triode. *Phys. Rev.*, 1948, 74(2):230.

15. Miller DA. Rationale and challenges for optical interconnects to electronic chips. *Proc. IEEE.*, 2000, 88(6):728-749.

16. Keyes RW. Physical limits in digital electronics. *Proc. IEEE.*, 1975, 63(5):740-767.

17. Pavesi L. Will silicon be the photonic material of the third millenium? *J. Phys.: Condens. Matter.*, 2003, 15(26):R1169.

18. Joannopoulos J, Johnson S, Winn J, Meade R. Photonic Crystals: Molding the Flow of Light-Second Edition. 2008, Princeton University Press.

19. Kitzerow HS, Matthias H, Schweizer SL, van Driel HM, Wehrspohn RB. Tuning of the optical properties in photonic crystals made of macroporous silicon. *Adv. Opt. Technol.*, 2008, 2008:780784.

20. Limonov MF, De La Rue R. Optical properties of photonic structures: interplay of order and disorder. 2019, CRC press.

21. Meade R, Winn JN, Joannopoulos J. Photonic crystals: Molding the flow of light. 1995, Pinceton University Press.

22. Nguyen TP, Tien TQ, Tong QC, Lai ND. An Optimization of Two-Dimensional Photonic Crystals at Low Refractive Index Material. *Crystals*, 2019, 9(9):442.

23. Lee W, Kim S, Kim S, Kim JH, Lee H. Hierarchical opal grating films prepared by slide coating of colloidal dispersions in binary liquid media. *J. Colloid Interface Sci.*, 2015, 440:229-235.

24. Kuo WK, Hsu JJ, Nien CK, Yu HH. Moth-eye-inspired biophotonic surfaces with antireflective and hydrophobic characteristics. *ACS Appl. Mater. Interfaces*, 2016, 8(46):32021-3030.

25. Nucara L, Piazza V, Greco F, Robbiano V, Cappello V, Gemmi M, Cacialli F, Mattoli V. Ionic strength responsive sulfonated polystyrene opals. *ACS Appl. Mater. Interfaces*, 2017, 9(5):4818-4827.

26. Nien CK, Yu HH. The applications of biomimetic cicada-wing structure on the organic light-emitting diodes. *Mater. Chem. Phys.*, 2019, 227:191-199.

27. Pennec Y, Djafari-Rouhani B, Vasseur JO, Larabi H, Khelif A, Choujaa A, Benchabane S, Laude V. Acoustic channel drop tunneling in a phononic crystal. *Appl. Phys. Lett.*, 2005, 87(26):261912.

28. Liu Z, Zhang X, Mao Y, Zhu Y, Yang Z, Chan CT, Sheng P. Locally resonant sonic materials. *Science*, 2000, 289(5485):1734-1736.

29. Yablonovitch E. Inhibited spontaneous emission in solid-state physics and electronics. *Phys. Rev. Lett.*, 1987, 58(20):2059.

30. Hulet RG, Hilfer ES, Kleppner D. Inhibited spontaneous emission by a Rydberg atom. *Phys. Rev. Lett.*, 1985, 55(20):2137.

31. Shi S, Chen C, Prather DW. Plane-wave expansion method for calculating band structure of photonic crystal slabs with perfectly matched layers. *J. Opt. Soc. Am. A.*, 2004, 21(9):1769-1775.

32. Johnson SG, Fan S, Villeneuve PR, Joannopoulos JD, Kolodziejski L. Guided modes in photonic crystal slabs. *Phys. Rev. B*, 1999, 60(8):5751.

33. Khelif A, Aoubiza B, Mohammadi S, Adibi A, Laude V. Complete band gaps in two-dimensional phononic crystal slabs. *Phys. Rev. E*, 2006, 74(4):046610.

34. Pennec Y, Rouhani BD, Li C, Escalante J, Martínez A, Benchabane S, Laude V, Papanikolaou N. Band gaps and cavity modes in dual phononic and photonic strip waveguides. *AIP adv.*, 2011, 1(4):041901.

35. Vasseur JO, Deymier PA, Djafari-Rouhani B, Pennec Y, Hladky-Hennion A. Absolute forbidden bands and waveguiding in two-dimensional phononic crystal plates. *Phys. Rev. B*, 2008, 77(8):085415.

36. Pennec Y, Djafari-Rouhani B, Larabi H, Vasseur J, Hladky-Hennion A. Low-frequency gaps in a phononic crystal constituted of cylindrical dots deposited on a thin homogeneous plate. *Phys. Rev. B*, 2008, 78(10):104105.

37. Wu T-T, Huang ZG, Tsai TC, Wu TC. Evidence of complete band gap and resonances in a plate with periodic stubbed surface. *Appl. Phys. Lett.*, 2008, 93(11):111902.

38. Saleh BEA, Teich MC. Fundamentals of photonics. 1991, p 313, Wiley-Interscience.

39. Kalra Y, Sinha R. Photonic band gap engineering in 2D photonic crystals. *Pramana*, 2006, 67(6):1155-1164.

40. Robinson S, Nakkeeran R. PCRR based bandpass filter for C and L+ U bands of ITU-T G. 694.2 CWDM systems. *Opt. Photonics J.*, 2011, 1(03):142.

41. Feit M, Fleck J. Computation of mode properties in optical fiber waveguides by a propagating beam method. *Appl. Opt.*, 1980, 19(7):1154-1164.

42. Yevick D, Bardyszewski W. Correspondence of variational finite-difference (relaxation) and imaginary-distance propagation methods for modal analysis. *Opt. Lett.*, 1992, 17(5):329-330.

43. Jungling S, Chen J. A study and optimization of eigenmode calculations using the imaginary-distance beam-propagation method. *IEEE J. Quantum Electron.*, 1994, 30(9):2098-2105.

44. Yevick D, Hermansson B. New formulations of the matrix beam propagation method: Application to rib waveguides. *IEEE J. Quantum Electron.*, 1989, 25(2):221-229.

45. Hadley GR, Smith R. Full-vector waveguide modeling using an iterative finite-difference method with transparent boundary conditions. *J. Lightwave Technol.*, 1995, 13(3):465-469.

46. Chen J, Jüngling S. Computation of higher-order waveguide modes by imaginary-distance beam propagation method. *Opt. Quantum Electron.*, 1994, 26(3):S199-S205.

How to cite this article: Sadeghfar F. Investigation and Comparison of Band Gap for Photon Crystals by Wave-Plate Method with Different Backgrounds. *Curr. Appl. Sci.*, 2023, 1(1):35-50. https://doi.org/10.22034/cas.2021.144387